

Predicted 3-D Structures for Mouse I7 and Rat I7 Olfactory Receptors and Comparison of Predicted Odor Recognition Profiles with Experiment

Spencer E. Hall, Wely B. Floriano, Nagarajan Vaidehi and William A. Goddard III

Materials and Process Simulation Center (MC: 139–74), California Institute of Technology, Pasadena, CA 91125, USA

Correspondence to be sent to: William A. Goddard, Materials and Process Simulation Center (MC: 139–74), California Institute of Technology, Pasadena, CA 91125, USA. e-mail: wag@wag.caltech.edu

Abstract

The first step in the perception of an odor is the activation of one or more olfactory receptors (ORs) following binding of the odorant molecule to the OR. In order to initiate the process of determining how the molecular level receptor-odorant interactions are related to odor perception, we used the MembStruk computational method to predict the three-dimensional (3-D) structure of the I7 OR for both mouse and rat. We then used the HierDock ligand docking computational method to predict the binding site and binding energy for the library of 56 odorants to these receptors for which experiment response data are now available. We find that the predicted 3-D structures of the mouse and rat I7 OR lead to predictions of odorant binding that are in good agreement with the experimental results, thus validating the accuracy of both the 3-D structure and the predicted binding site. In particular we predict that heptanal and octanal both bind strongly to both mouse and rat I7 ORs, which conflicts with the older literature but agrees with recent experiments. To provide the basis of additional validations of our 3-D structures, we also report the odorant binding site for a new odorant (8-hydroxy-octanal) with a novel functionality designed to bind strongly to mouse I7. Such validated computational methods should be very useful in predicting the structure and function of many other ORs.

Key words: G protein coupled receptor, hydrogen bonds, molecular dynamics; transmembrane domain

Introduction

The early stage in odorant detection involves binding of the odorant molecule to an olfactory receptor (OR; Buck and Axel, 1991; Lancet *et al.*, 1993) followed by activation of the OR through release of the G-protein fragments. Each olfactory sensory neuron expresses only one OR type, but a particular OR can respond to multiple odorants. A particular ligand can also elicit response from multiple ORs. This leads to a unique combination of OR responses for each odorant (Malnic *et al.*, 1999). Thus the mammalian olfactory system uses a combinatorial response to discriminate thousands of odorants (Sicard and Holley, 1984; Malnic *et al.*, 1999; Kajiya *et al.*, 2001).

ORs belong to the superfamily of membrane bound G-protein coupled receptors (GPCRs; Buck and Axel, 1991; Mombaerts, 1999). There are 913 ORs in mice (Godfrey *et al.*, 2004) and 339 ORs in humans (Malnic *et al.*, 2004) making it an extremely forbidding task to elucidate experimentally (or computationally) the details by which odorants activate each of the ORs. There is almost no molecular level information on how and where each odorant binds to the OR or when and how this leads to their activation. The

major impediment to obtaining this molecular level information is that there is no experimental three-dimensional (3-D) structural information available for any OR of any species of life! Indeed, considering all forms of life, there is an experimental 3-D structure for only a single GPCR, bovine rhodopsin (Grigorieff *et al.*, 1996). This is because it has not yet been possible to obtain crystals suitable for diffraction studies of these membrane bound proteins, despite years of intense effort.

Consequently, we have developed computational techniques (MembStruk) suitable for predicting the 3-D structures of GPCRs. The original version of MembStruk1.0, was validated on bacteriorhodopsin and used for prediction of structure of OR-S25 (Floriano *et al.*, 2000). Subsequent improved version of MembStruk2.0 (with optimization of rotational orientations of the helices) have been validated for bovine rhodopsin, where it leads to a CRMS (coordinate root-mean-square) error of 2.8 Å in the transmembrane (TM) domains (Vaidehi *et al.*, 2002; Trabanino *et al.*, 2004) compared to the crystal structure (Poincelot *et al.*, 1970; Palczewski, 2000). We have also validated the

MembStruk2.0 predicted structures for human $\beta 1$ and $\beta 2$ adrenergic receptors (Vaidehi *et al.*, 2002; Freddolino *et al.*, 2004) and human dopamine D2 receptor (Kalani *et al.*, 2004). Since no experimental structural data are available for direct validation of our predicted structures for these systems, we used the HierDock2.0 method (Floriano *et al.*, 2000; Vaidehi *et al.*, 2002) to predict the binding sites of ligands to the predicted 3-D structures of these GPCRs. These binding sites were then compared to the numerous experimental mutation and binding studies carried out in developing subtype specific agonist and antagonist pharmaceuticals. We found that the predicted binding site of these ligands all agree quite well with all available experimental mutation data. This validation of the techniques gives us confidence to now apply these techniques (MembStruk and HierDock) to the more complex problem of ORs, where all available information suggests much less selectivity than for the rhodopsin, adrenergic and dopamine receptors.

There has been some progress in determining which odorants lead to activation of specific mammalian ORs. However, the experiments are laborious and results are available on only a few ORs for a relatively small library of odorants (Kiefer *et al.*, 1996; Bozza and Kauer, 1998; Krautwurst *et al.*, 1998; Zhao *et al.*, 1998; Duchamp-Viret *et al.*, 1999; Malnic *et al.*, 1999; Mori *et al.*, 1999; Rubin and Katz, 1999; Araneda *et al.*, 2001; Kajiya *et al.*, 2001). Consequently, we have chosen to apply the MembStruk and HierDock methods to these few more well studied ORs as the first step in approaching the much more complicated task of elucidating the structures and function for the whole set of mammalian ORs.

Our first report on the structure and ligand binding for an OR (Floriano *et al.*, 2000) was for the S25 mouse OR where it was known that only 2 of 24 simple aliphatic odorants were agonists for this ORS25. Here, we correctly predicted that the two known cases do bind much more strongly than the other 22 odorants and report a more complete validation by comparing the calculated binding energies of 56 odorants to the intracellular Ca^{2+} imaging measurements to the rat and mouse I7 OR. Prior to publication of these experimental results (Bozza *et al.*, 2002), we arranged to carry out a blind test of our methods. Tom Bozza and Peter Mombaerts (Rockefeller University) sent us the names of the 56 odorants (shown in Table 1) for which they had measured the intracellular calcium influx response for the I7 OR both rat and mouse, but they provided no experimental data until after we reported to them our calculated binding sites and energies, reported herein. We predicted the structure and odorant binding energies of R-I7 and M-I7 using MembStruk1.0 and HierDock2.0. They then provided us with the list of experimental agonists for these two ORs, which then was published (Bozza *et al.*, 2002). As shown in this paper, the calculated binding energies correlate well, but not perfectly to the experimental activation profiles (correctly showing that binding to aldehydes is favored

while binding to such chemical classes as acids and alcohols are not favored). In addition our predictions confirmed in advance the result that both rat and mouse I7 receptor are activated by both heptanal and octanal.

After making these blind predictions, we made significant improvements to the MembStruk structure prediction methods for our studies on biogenic amine receptors, where there are large amounts of experimental data on mutations and ligand binding affinities. These improved methods have now been applied to mouse and rat I7 ORs, leading to results that are in significantly improved agreement with experimental measurements of the intracellular calcium imaging results. Based on our best predictions of the structure and binding site, we have designed three new odorants with two functional groups that we predict will bind to mouse and rat I7 receptors. Experimental tests on these compounds would provide additional tests on how well the theory can be trusted for predictions prior to experiment.

The mouse I7 (M-I7) and rat I7 (R-I7) ORs both contain 301 residues. They have 95% sequence identity, differing by only 15 residues, four of which are located in the TM region (see Figure 1). Despite the high similarity of M-I7 and R-I7, their odorant activities are somewhat different (Krautwurst *et al.*, 1998; Zhao *et al.*, 1998; Wetzel *et al.*, 1999; Araneda *et al.*, 2000; Bozza *et al.*, 2002; Levasseur *et al.*, 2003). These differences and similarities in odor recognition make M-I7 and R-I7 good candidates to test how well our modeling techniques can discriminate odor differentiation resulting from slight changes in sequence. Previous modeling of R-I7 based on bacteriorhodopsin structure was reported by Singer (2000).

Results and discussion

We report here the predictions for the 3-D atomic-level structures of the M-I7 and R-I7 ORs, the binding sites for the odorants that activate these receptors and the relative binding energies for the odorants in these sites. We find results that correlate well with the experimental intracellular calcium ion influx measurements (Araneda *et al.*, 2000; Bozza *et al.*, 2002; T. Bozza, personal communication).

Prediction of the 3-D structure of M-I7 and R-I7 ORs

The details of the methods used for predicting the structure and function of M-I7 and R-I7 ORs are described in an appendix (see Supplementary material). However, in the next section a brief outline of the methods as applied to M-I7 and R-I7 are given.

Predicted structures for M-I7 and R-I7

To predict the TM regions we aligned the sequences for M-I7 and R-I7 along with 21 other rat and mouse ORs that had similar homology and these alignments were used to predict the TM region based on hydropathicity profiles (Trabanino *et al.*, 2004). The predicted TM regions for M-I7 are

Table 1 Odorants studied with theory and experiment

Ligands	Mixtures in Bozza <i>et al.</i> (2002)	Main functional group	Ligands	Mixtures in Bozza <i>et al.</i> (2002)	Main functional group
1-Decanol	A	Alcohol	Benzaldehyde	D	Aldehyde
2-Phenylethanol	A	Alcohol	Butyraldehyde	D	Aldehyde
Butanol	A	Alcohol	Decanal	D	Aldehyde
Citronellal (–)	A	Aldehyde	Hexanal	D	Aldehyde
Citronellal (+)	A	Aldehyde	Lilial	D	Aldehyde
Geraniol	A	Alcohol	Lylal	D	Aldehyde
Hexanol	A	Alcohol	Octanal	D	Aldehyde
Linalool (–)	A	Alcohol	<i>Trans</i> -cinnamaldehyde	D	Aldehyde
Linalool (+)	A	Alcohol	Allyl phenoxylacetate	E	Ester
Octanol	A	Alcohol	Amyl butyrate	E	Ester
Benzyl propionate	B	Ester	Ethyl acetate	E	Ester
Butyric acid	B	Carboxylic acid	Heptyl butyrate	E	Ester
Decanoic acid	B	Carboxylic acid	Hexyl acetate	E	Ester
Ethyl benzoate	B	Ester	<i>n</i> -Butyl acetate	E	Ester
Hexanoic acid	B	Carboxylic acid	Octyl acetate	E	Ester
Octanoic acid	B	Carboxylic acid	Propyl butyrate	E	Ester
Phenethylamine	B	Amine	2-Butanone	F	Ketone
Propionic acid	B	Carboxylic acid	2-Hexanone	F	Ketone
2-Sec-butylcyclohexanone	C	Ketone	2-Octanone	F	Ketone
Estragole	C	Ester	Acetophenone	F	Ketone
Eucalyptol	C	Ether	Beta-ionone	F	Ketone
Eugenol	C	Alcohol	Ethylisoamylketone	F	Ketone
Isopulegol	C	Alcohol	Ethylvanillin	F	Aldehyde
Menthone_1	C	Ketone	Hedione	F	Ketone
Menthone_2	C	Ketone	2–4-Dimethylacetophenone	NR	Ketone
Menthone_3	C	Ketone	2-Aminoacetophenone	NR	Ketone
Menthone_4	C	Ketone	Butyrophenone	NR	Ketone
R-neg-carvone	C	Ketone	Citral	NR	Aldehyde
S-pos-carvone	C	Ketone	Heptanal	NR	Aldehyde
			Nonanal	NR	Aldehyde
			Propiophenone	NR	Ketone
			Valeraldehyde	NR	Aldehyde
			Valerophenone	NR	Ketone

There are 62 stereoisomers (56 molecules). The experiments involved coarse sampling of seven mixtures (A–NR) which were examined individually for those mixtures that led to a positive

compared in Figure 1. Using the predicted TM regions, we applied the MembStruk1.0 method to predict the 3-D

structures. Two sets of structures were predicted using MembStruk1.0 and subsequently MembStruk2.0 methods.

I7-Mouse NT	1	MERRNHTGRVSEFVLLGFPAPAPLRA	26	I7-Mouse LP4 (E)	170	RLSYCGPNTINHFFCDVSPLLNLSCDTMSTAE	201
I7-Rat NT	1	MERRNHSGRVSEFVLLGFPAPAPLRV	26	I7-Rat LP4 (E)	170	RLSYCGPNTINHFFCDVSPLLNLSCDTMSTAE	201
I7-Mouse TM1	27	LLFFLSLLAYVLVTENILIIITAI	50	I7-Mouse TM5	202	LTDFILAIIFILLGFLSVTGASYM	224
I7-Rat TM1	27	LLFFLSLLAYVLVTENMLIIITAI	50	I7-Rat TM5	202	LTDFVLAIIFILLGFLSVTGASYM	224
I7-Mouse LP1 (I)	51	RNHPTLHK	58	I7-Mouse LP5 (I)	225	AITGAVMRIPSAAGR	240
I7-Rat LP1 (I)	51	RNHPTLHK	58	I7-Rat LP5 (I)	225	AITGAVMRIPSAAGR	240
I7-Mouse TM2	59	PMYFFLANMSFLEIWTVTIP	80	I7-Mouse TM6	241	KAFSTCASHLTVVIIFYAASIFIYA	265
I7-Rat TM2	59	PMYFFLANMSFLEIWTVTIP	80	I7-Rat TM6	241	KAFSTCASHLTVVIIFYAASIFIYA	265
I7-Mouse LP2 (E)	81	KMLAGFIGSEENHGQLISFEACMT	104	I7-Mouse LP6 (E)	266	RPKALSAPDTNK	277
I7-Rat LP2 (E)	81	KMLAGFIGSKENHGQLISFEACMT	104	I7-Rat LP6 (E)	266	RPKALSAPDTNK	277
I7-Mouse TM3	105	QLYFFLGLGCTECVLLAVMAYDRY	128	I7-Mouse TM7	278	LVSVLYAVIVPLNPIIYC	296
I7-Rat TM3	105	QLYFFLGLGCTECVLLAVMAYDRY	128	I7-Rat TM7	278	LVSVLYAVIVPLNPIIYC	296
I7-Mouse LP3 (I)	129	VAICHPLHYFVIVSSR	144	I7-Mouse CT	297	LRNQEVKALERTLHLAQGDANTKSSRDG	327
I7-Rat LP3 (I)	129	VAICHPLHYFVIVSSR	144	I7-Rat CT	297	LRNQDVKALERTLHLAQDEANTNKGSKIG	327
I7-Mouse TM4	145	LCVQMAAGSWAGGFGISMVKVFLIS	169				
I7-Rat TM4	145	LCVQMAAGSWAGGFGISMVKVFLIS	169				

Figure 1 The sequence alignments of I7 mouse and I7 rat where (I) is for intracellular loops and (E) is for extracellular loops. Residues that are different in M-I7 and R-I7 are marked with an 'M'. The residues within 3.5 Å of the ligands on the final improved models are marked with a 'B'. For M-I7 and R-I7, there are no sequence differences in the binding region. Based on alignment studies, Krautwurst *et al.* (1998) had suggested that residue 206 (Ile for M-I7 and Val for R-I7) is involved in binding; however, our predicted 3-D structure puts this residue far from the binding pocket.

The first structures using MembStruk1.0 (described in Floriano *et al.*, 2000) are denoted as preM-I7 and preR-I7. These structures were used for the predictions made in the blind study, prior to the publication of the experimental odorant activation assays (Bozza *et al.*, 2002). Subsequently, the improved version of MembStruk2.0 method was used, as described in an Appendix (<http://www.wag.caltech.edu/gpcr/i7/appendix.html>) and in Vaidehi *et al.* (2002), to obtain the final structures of M-I7 and R-I7. These improvements in MembStruk2.0 used the calculated potential energy to determine the optimum rotational orientation of the helices, rather than just the hydrophobic moment as in MembStruk1.0. These were motivated by studies we were doing on the structures of dopamine and adrenergic receptors (Freddolino *et al.*, 2004; Kalani *et al.*, 2004). In addition, we used the predicted structure of M-I7 and the high sequence homology between R-I7 and M-I7 to build a homology model for R-I7 based on the predicted M-I7 structure as template. Below we refer to this as the R-I7(hom) structure.

For each of these 3-D structures we applied HierDock2.0 (Vaidehi *et al.*, 2002) to predict the odorant binding sites and binding energies of the 62 molecule odorant library. Since the results using as preM-I7 and preR-I7 were obtained prior to knowledge of the experimental results, we consider it valuable to report them here. Hence, the methods used to these results are described in detail in an appendix (<http://www.wag.caltech.edu/gpcr/i7/appendix.html>). However, the main body of the results and the analysis of the binding sites have been done with the predictions with R-I7(hom) and M-I7 that are in better agreement with experiment.

Comparison of the Predicted M-I7 and R-I7(hom) Structures

A standard way to compare different structures for the same protein is to determine the coordinate root-mean-square (CRMS) difference between the structures (after matching the center of mass and moments of inertia). However, since CRMS is an average quantity it does not have the discrimination required to understand how the differences in structure might affect function. Consequently, we developed the 'MembComp' method for comparing the structural features of two GPCRs. Here, we start with the reference plane intersecting hydrophobic center (Trabanino *et al.*, 2004) of each TM helix of the final structure, compare such helical characteristics as helical bends and tilts (Filizola *et al.*, 1998; Trabanino *et al.*, 2004) for each of the 7 TM domains. These helical properties are summarized in Table 2 and Figure 2. These results show that the M-I7 and R-I7(hom) structures are remarkably similar with only slight differences in their hydrophobic moments, as expected by the 95% sequence identity. The main chain atoms in the TM region differ by a CRMS of only 1.5 Å.

Table 3 compares the structural features between M-I7 and bovine rhodopsin (which have a sequence identity of 11%), while Figure 2 compares them graphically. The CRMS difference between these structures is 6.22 Å, with the largest differences in the hydrophobic moments of TM6 and a salt bridge from TM6 to the IC2 loop in rhodopsin. With such a large difference in structure, we expect that using bovine rhodopsin as the template for homology structure predictions may not lead to useful predicted structures for the ORs.

Table 2 The calculated structural features of the M-I7 and R-I7(hom) final structures

	Mouse I7 Structural information				Rat I7 (hom) Structural information			
	Helical bend	Helical tilt	HPM angle	Helical translation	Helical bend	Helical tilt	HPM angle	Helical translation
Helix 1	2.7	23.8	−96.8	0.229	2.5	23.8	−104.9	0.230
Helix 2	11.4	28	−20.7	−0.088	11.4	28	−20.6	−0.086
Helix 3	7.2	25	−54.3	−0.298	7.2	25	−74.7	−0.294
Helix 4	4.7	2.6	−36.8	0.037	4.7	2.6	−36.9	−0.038
Helix 5	15.2	17	142.7	0.376	15.2	17	156.7	0.374
Helix 6	4.8	9.2	110.5	0.173	4.8	9.2	110.7	0.169
Helix 7	25	21.4	13.8	0.010	25.3	21.4	17.4	0.017

The helical bend is defined as 180° minus the angle between the tips of the helix and its middle, so that the larger the angle the more it deviates from being perfectly straight. The helical tilt is 90° minus the angle the helix makes with respect to the intersecting plane (MembComp), so that a helix with a tilt of 0° is perpendicular to the membrane. The hydrophobic moment angle is calculated from the projection of the Eisenberg hydrophobicity (Eisenberg et al., 1984) of the middle 15 residues of the helix onto the plane perpendicular to the helix; here zero points 180° away from the center point of the protein; positive angles have this hydrophobicity vector rotating counter-clockwise on the plane (top view looking down from the extracellular region). Helical translation is the distance in angstroms that the geometric center of the helix is from the plane of intersection.

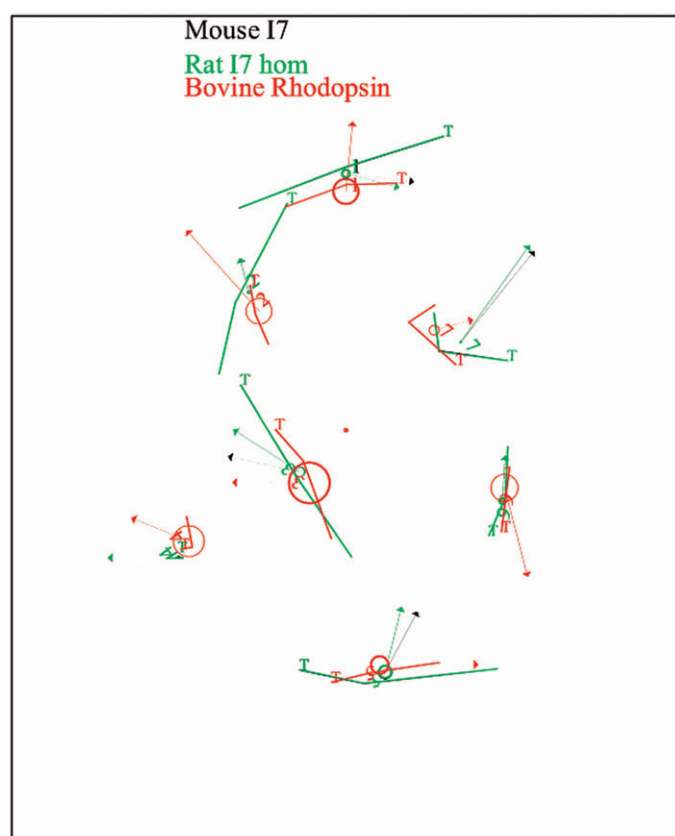


Figure 2 Shown is the top view (looking down from the extracellular region) of the alignment of structures M-I7, R-I7(hom) and bovine rhodopsin on the plane of intersection through their centers of hydrophobicity. The center point is the center of mass of both structures and the circles represent the distance of the helix from the plane (a thicker circle is upwards towards the extracellular region). The arrows represent the hydrophobic moment of the helices.

Table 3 Comparison of structural features of the predicted structure for mouse I7 with the X-ray crystallography results for bovine rhodopsin

	Diff. in helical bend	Diff. in helical tilt	Diff. in HPM angle	Diff. in helical translation
Helix 1	6.7	1.1	−91.2	−0.521
Helix 2	4.6	15.5	−26.2	0.682
Helix 3	1	2	1.4	−1.521
Helix 4	20.2	1.7	20.7	0.963
Helix 5	8.6	4.9	60.6	−0.152
Helix 6	23	15.4	165.9	0.980
Helix 7	7.6	4.8	47.4	0.311

These numbers are derived by comparing the predicted numbers for the M-I7 structure with the values in Table 2 for bovine rhodopsin. Here, the difference is (M-I7 minus bovine rhodopsin). The numbers from bovine rhodopsin were obtained using the hydrophobic centers (Trabanino et al., 2004) of each helix to center the plane of intersection and the middle 15 residues about that center.

Experimental methods to determine odorant activation profiles

The odorant activation profiles for the M-I7 and R-I7 ORs were determined experimentally by Dr Tom Bozza of Rockefeller University, using fura-2 calcium imaging in acutely dissociated olfactory sensory neurons. KCl and forskolin were used as positive control stimuli (see Bozza et al., 2002). These experiments were carried out by first grouping the odorants into six sets or mixtures (A–F) as shown in Table 1. Then for those mixtures with a positive response, the mixtures were separated into individual components to

determine which odorant was causing the activation of the OR (Bozza *et al.*, 2002). We had no access to these experimental results, nor did we make use of literature data (Araneda *et al.*, 2000), until the predictions of binding energies using the preM-I7 and preR-I7 predicted structures were completed and sent to Bozza.

Predicted binding site and binding energy for odorants in M-I7 and R-I7 ORs

Identification of the putative odorant binding site

We predicted the putative binding site for each of the 62 test odorants to both R-I7 and M-I7, by using HierDock2.0 to scan the entire receptor structure. The first step was to partition the entire receptor into 13 overlapping binding regions containing all the internal voids and surface accessible voids present in the predictions protein structures. Then we applied the HierDock2.0 protocol, described in Vaidehi (2002) and summarized in an Appendix (<http://www.wag.caltech.edu/gpcr/i7/appendix.html>), to docking the potential odorants to each of these regions. The best binding region of these 13 regions for all of the test odorants was found to be located between TM helices, 3, 4, 5 and 7 in both the OR structures.

Binding energies of odorants in the preM-I7 and preR-I7 structures

Having located the binding region, the HierDock2.0 protocol (detailed at <http://www.wag.caltech.edu/gpcr/i7/appendix.html>) was again used to dock all 62 odorants in this putative binding region for both M-I7 and R-I7 and to calculate the binding energy. The calculated binding energies of odorants in the initial preR-I7 and preM-I7 structures are shown in Table 4. The odorants with the best binding energies have their energies shaded darkest (predicted binding energy greater than 30 kcal/mol, none seen in this table) while the second best are shaded lightest (predicted binding energies >25 kcal/mol and <30 kcal/mol), followed by (for 20–25 kcal/mol) and (for 15–20 kcal/mol). As indicated in Table 4, the pattern of predicted binding energies is in fair agreement with experimental intracellular calcium concentration measurements for both R-I7 and M-I7 structures. For example, we predicted that both heptanal and octanal bind strongly to both M-I7 and R-I7 in disagreement with the published experiments (Krautwurst *et al.*, 1998), but as we learned later this does agree with the new experiments (Bozza *et al.*, 2002). Overall, 25% of the odorant predicted to be good binders (shaded lightest) were confirmed by experiment, while 17% of the odorants with medium affinity predictions were confirmed, 10% of the weak binding odorants and 7% of the unmarked were observed to be agonists. Comparison of the calculated binding energies to the experimental data available in literature (Araneda *et al.*, 2000; Levasseur *et al.*, 2003), we find that 50% of the good binding odorants (shaded lightest) are

also found to be agonists with experiments. For example, nonanal and decanal were shown to be agonists for R-I7 (Araneda *et al.*, 2000; Levasseur *et al.*, 2003), which is in agreement with the calculated binding energies in Table 4. The blind predictions correctly concluded that aldehydes would be the main group activating R-I7 and M-I7.

Binding energies of the odorants in the R-I7(hom) and M-I7 refined structures

Although the MembStruk1.0 calculations led to results in fair agreement with the measured activation profiles for R-I7 and M-I7 receptors, there were several false positives (e.g. linal, lylal and benzaldehyde) in the prediction. Later, the MembStruk1.0 method was improved while we were predicting the structure and function for the dopamine and adrenergic receptors, for which there is abundant mutation data available to validate the predicted binding sites.

After completing the computational results in the blind test, we applied the improved MembStruk2.0 method to again predict the 3-D structures of the I7 receptors. Then we used these new I7 structures with HierDock2.0 to predict the binding site and binding energy for the 62 odorants. The calculated binding energies of the odorants for the improved structures are shown in Table 5.

To simplify comparisons the calculated binding energies of the 62 ligands were categorized into seven grades. They are: class A, the best binding odorants with binding energies ranging from 30 to 40 kcal/mol (energies shaded darkest in Tables 4 and 5); class B (25–30 kcal/mol; shaded lightest); class C (20–25 kcal/mol); class D (15–20 kcal/mol); class E (10–15 kcal/mol no color); class F (0–10 kcal/mol, no color); and class G, negative binding energy indicating no binding, no color.

Comparing to experiment (see Table 5) we find the following.

- Among class A, M-I7 has six aldehydes (of which four were observed experimentally to be agonists) and one ketone (not an agonist experimentally). While R-I7 has five aldehydes, of which all but decanal were observed experimentally to be agonists by Bozza, while decanal was also observed to be agonist by Araneda *et al.* (2000) and one ester (not an agonist experimentally).
- Among class C, M-I7 has one alcohol, four esters and three ketones none of which were observed to be agonists experimentally, while R-I7 has four aldehydes, two alcohols, two esters and three ketones, none of which were agonists.
- Among classes D–G, were the other 38 odorants for M-I7 and 37 odorants for R-I7, none of which were observed to be agonists.

Overall there is good agreement between the calculated binding energies and measured intracellular calcium

Table 4 Predicted binding energies (bindE) for 62 odorants docked to preM-I7 and preR-I7 (initial structures from MembStruk 1.0)

Main functional group	preM-I7		PreR-I7	
	Odorants	Binding energy	Binding energy	Odorants
Alcohols	Eugenol	23.3549	25.4398	Linalool_2
	Geraniol	21.8517	23.9436	Isopulegol
	1-Decanol	20.1559	23.5012	Hexanol
	Hexanol	18.8009	22.5973	Geraniol
	2-Phenylethanol	18.1569	21.7624	Eugenol
	Linalool_2	14.2584	21.1655	1-Decanol
	Octanol	14.0985	20.7105	Octanol
	Linalool_1	13.5163	18.239	2-Phenylethanol
	Butanol	13.0441	16.8347	Linalool_1
Aldehydes	Isopulegol	12.1976	9.1033	Butanol
	Heptanal	20.1688	28.369	Lilial
	Octanal	19.8699	28.1088	Lylal
	Trans-cinnamaldehyde	19.5762	28.0253	Octanal
	Citral	19.541	27.903	Nonanal
	Benzaldehyde	19.3014	27.0856	Trans-cinnamaldehyde
	Hexanal	18.7467	26.387	Decanal
	Valeraldehyde	17.2835	23.0211	Citronellal_2
	Lilial	16.403	23.021	Citronellal_1
	Butyraldehyde	16.3906	21.8599	Heptanal
	Citronellal_1	15.3972	17.7824	Hexanal
	Nonanal	12.7425	15.1777	Benzaldehyde
	Ethylvanillin	12.1059	14.8358	Citral
	Decanal	6.9409	13.9503	Ethylvanillin
	Lylal	6.6487	13.491	Valeraldehyde
	Citronellal_2	3.4479	13.4052	Butyraldehyde
Amine	Phenethylamine	18.9052	18.3947	Phenethylamine
Carboxylic acids	Decanoic acid	-28.0902	-21.0831	Octanoic acid
	Propionic acid	-32.3476	-23.7293	Decanoic acid
	Butyric acid	-33.7047	-32.4055	Propionic acid
	Hexanoic acid	-36.6969	-34.6077	Butyric acid
	Octanoic acid	-44.3261	-46.075	Hexanoic acid
Esters	Estragole	22.4664	26.8226	Allyl phenoxyacetate
	Heptyl butyrate	22.4269	22.7531	Octyl acetate
	Benzyl propionate	22.3856	22.0913	Benzyl propionate
	Allyl phenoxyacetate	21.4895	21.9963	Heptyl butyrate
	Hexyl acetate	18.0473	20.2049	Estragole
	Ethyl benzoate	17.5044	17.7453	Amyl butyrate
	Octyl acetate	15.3891	17.7056	Ethyl benzoate

Experimentally obs.

Exper. not tested

Table 4 Continued

Main functional group	preM-I7	PreR-I7		
	Odorants	Binding energy	Binding energy	Odorants
Esters	Amyl butyrate	14.185	15.3482	Hexyl acetate
	<i>n</i> -Butyl acetate	13.6357	15.2579	<i>n</i> -Butyl acetate
	Propyl butyrate	11.8501	13.7925	Propyl butyrate
	Ethyl acetate	10.8684	10.9677	Ethyl acetate
Ether	Eucalyptol	13.8212	16.8397	Eucalyptol
Ketones	Hedione	19.5438	23.7739	Hedione
	S-pos-carvone	19.448	22.057	Valerophenone
	Valerophenone	19.1377	20.0833	Menthone_4
	2-Aminoacetophenone	18.2872	19.1754	S-pos-carvone
	Menthone_4	18.0405	18.7952	Menthone_1
	R-neg-carvone	17.9541	18.697	Butyrophenone
	Butyrophenone	17.8733	18.6434	Menthone_3
	Acetophenone	16.9442	18.632	2-Sec-butylcyclohexanone
	Menthone_3	16.8149	18.5699	R-neg-carvone
	Menthone_2	16.2458	18.4417	2-4-Dimethylacetophenone
	Propiophenone	16.019	18.4151	Menthone_2
	2-Sec-butylcyclohexanone	15.2167	17.0927	Propiophenone
	Ethylisoamylketone	15.1637	16.7109	2-Aminoacetophenone
	2-Octanone	14.9939	16.6653	Ethylisoamylketone
	2-4-Dimethylacetophenone	14.9734	16.4814	Acetophenone
	Menthone_1	13.4099	14.6461	2-Octanone
	2-Hexanone	13.134	14.1881	2-Butanone
	2-Butanone	8.8244	13.8867	Beta-ionone
	Beta-ionone	1.791	13.4883	2-Hexanone

The binding energies (in kcal/mol) were calculated as the difference between the energy of the ligand in protein and in solution. The solvation corrections were calculated using the analytical volume generalized Born (AVGB) continuum solvation approach (Rappé and Goddard, 1991; Ghosh *et al.*, 1998; Zamanakos, 2001). Dark shaded ligand names are those that experimentally tested positive for being an agonist. Note that these are the results that were predicted prior to knowing the experimental results but they are not our final predicted binding energies for the best OR structures, which are shown in Table 5.

response. Thus 62% (69% including decanal in I7 rat) of class A odorants were observed to be agonists experimentally, while 33% (39% including nonanal in I7 rat) of class B odorants and none of the five lower binding classes (with 75% of the odorants) were observed to be agonists. Clearly, the predictions identified aldehydes as the prominent binders to I7, which correlates well with the experimental observation that only aldehydes activate these ORs. Most of

the experimental agonists (56% including decanal and nonanal for I7 rat) are in the top predicted binders shaded darkest (predicted binding energy >30 kcal/mol). The rest of the experimental agonists (44%) are the next best binders shaded lightest.

The false positives in the calculations could be due to (i) inaccuracies in the calculation of the binding energies such as no explicit inclusion of entropy or room temperature

Table 5 Calculated binding energies (bindE in kcal/mol) for 62 odorants docked to M-I7 and R-I7(hom) (MembStruk 2.0)

Main functional group	M-I7		R-I7 (hom)	
	Odorants	Binding energy	Binding energy	Odorants
Alcohols	1-Decanol	25.833	28.0723	Eugenol
	Geraniol	23.394	20.2245	Geraniol
	Linalool (–)	19.4196	20.1064	2-Phenylethanol
	Linalool (+)	19.3595	19.1402	Linalool (+)
	Isopulegol	18.8207	18.8096	Linalool (–)
	Eugenol	18.8195	17.295	Isopulegol
	Octanol	18.0531	16.9033	Octanol
	2-Phenylethanol	15.2703	14.9007	Hexanol
	Hexanol	14.0971	14.1861	1-Decanol
	Butanol	11.3627	9.9988	Butanol
Aldehydes	Citronellal (+)	36.3917	37.6058	Citronellal (+)
	Citronellal (–)	35.349	34.4672	Octanal
	Octanal	34.6702	32.8259	Citronellal (–)
	Lilial	33.1472	31.9751	Heptanal
	Heptanal	32.0736	30.5379	Decanal
	Lylal	31.4951	29.4017	Hexanal
	Hexanal	29.6216	28.9095	Citral
	Trans-cinnamaldehyde	29.5612	28.8805	Trans-cinnamaldehyde
	Decanal	29.2197	27.5458	Nonanal
	Nonanal	28.3484	26.8598	Valeraldehyde
	Citral	27.9483	26.67	Benzaldehyde
	Valeraldehyde	27.2348	24.667	Butyraldehyde
	Benzaldehyde	25.7413	24.5735	Ethylvanillin
	Butyraldehyde	25.1915	24.1046	Lilial
	Ethylvanillin	17.9797	23.3419	Lylal
	Phenethylamine	16.4163	16.7974	Phenethylamine
	Octanoic acid	–48.8842	–45.3474	Octanoic acid
Carboxylic acids	Decanoic acid	–50.1171	–49.6298	Decanoic acid
	Butyric acid	–51.5923	–50.3061	Hexanoic acid
	Hexanoic acid	–54.4322	–53.7466	Butyric acid
	Propionic acid	–56.2012	–57.0789	Propionic acid
	Heptyl butyrate	24.3095	31.6391	Heptyl butyrate
Esters	Hexyl acetate	23.4023	21.1906	Estragole
	Estragole	21.4444	20.2919	Amyl butyrate
	Allyl phenoxyacetate	20.4052	19.5893	Allyl phenoxyacetate
	Benzyl propionate	19.8806	19.4513	Benzyl propionate
	Octyl acetate	19.6909	16.3143	Ethyl benzoate
	Amyl butyrate	19.0082	16.2418	Octyl acetate

Experimentally obs.

Exper. not tested

Table 5 Continued)

Main functional group	M-I7	R-I7 (hom)		
	Odorants	Binding energy	Binding energy	Odorants
Esters	Ethyl benzoate	17.3801	16.0278	<i>n</i> -Butyl acetate
	<i>n</i> -Butyl acetate	16.662	14.1957	Hexyl acetate
	Ethyl acetate	15.2516	14.1143	Propyl butyrate
	Propyl butyrate	12.0733	12.7487	Ethyl acetate
Ether	Eucalyptol	16.2489	17.3514	Eucalyptol
Ketones	Hedione	34.279	25.1749	2-Aminoacetophenone
	S-pos-carvone	24.0873	24.4053	S-pos-carvone
	R-neg-carvone	21.0394	22.334	Valerophenone
	Valerophenone	20.4357	20.0365	Hedione
	Menthone_4	19.9672	19.3576	Menthone_4
	Menthone_2	19.0371	18.4258	Menthone_2
	Butyrophenone	18.9148	18.2823	Menthone_1
	2-4-Dimethylacetophenone	18.2875	18.2542	2-4-Dimethylacetophenone
	2-Aminoacetophenone	18.1204	17.8611	Propiophenone
	Propiophenone	17.4388	17.8608	Ethylisoamylketone
	Menthone_1	17.328	17.7167	Menthone_3
	2-Sec-butylcyclohexanone	16.5561	16.7056	Butyrophenone
	Ethylisoamylketone	16.4425	16.378	2-Sec-butylcyclohexanone
	Acetophenone	16.1283	15.959	Acetophenone
	Menthone_3	14.4766	14.3462	2-Octanone
	2-Octanone	14.1908	13.9042	R-neg-carvone
	2-Hexanone	13.0558	12.6953	2-Hexanone
	2-Butanone	9.2929	11.7602	Beta-ionone
	Beta-ionone	-4.8323	11.2887	2-Butanone

Each binding energy was calculated as the difference between the energy of the ligand in protein and in solution. The solvation corrections were calculated using the analytical volume generalized Born (AVGB) continuum solvation approach (Rappé and Goddard, 1991; Ghosh *et al.*, 1998; Zamanakos, 2001). Dark shaded ligand names are those that experimentally tested positive for being an antagonist.

effects or (ii) the fact that some of these odorants predicted as false positives do bind but may not activate the ORs and could act as antagonists.

The available experimental data involves measuring the increase in calcium ion concentration in individual olfactory sensory neurons, which is a measure of activation by the odorant and not just the binding whereas the theory calculates binding site and binding energy of the odorant but not the activation process of the ORs. Strong binding is a necessary but not a sufficient condition for activation and hence our calculated binding energies should best be compared to measured binding constants. Unfortunately, such data is scarce and are not yet available for these mammalian ORs.

Thus some odorants predicted to have good binding energies may not bind in the correct configuration to activate the OR serving perhaps as an antagonist rather than an agonist.

For example, we predict lilial and lyral to be in the top (red) group of good binders, whereas the experiments did not find them to activate the receptors (Bozza *et al.*, 2002). There are two possible explanations for this discrepancy between binding energy and measured activation: (i) the experiments tested these odorants only in a mixture; this makes the comparison of theory with experiment ambiguous, since a mixture might contain an antagonist ligand that would compete with an agonist in the mixture; and (ii) the other possibility is that lilial and lyral themselves could

be antagonists to these rat and mouse I7 ORs. In the third section, we discuss competitive binding experiments that could test if some odorants predicted to be top binders are not observed to activate because they are antagonists or because that are agonists but inhibited by antagonists.

Residues predicted to be directly involved in binding of odorants to the R-I7 and M-I7 OR structures

Figure 3 shows the predicted binding sites for octanal in M-I7 and R-I7(hom). Octanal was predicted as a good binder and shown experimentally to be an agonist for both M-I7

and R-I7 (Araneda *et al.*, 2000; Bozza *et al.*, 2002). Figure 3A,C indicate the binding pocket depth as ~ 10 Å deep from the extracellular surface. This is similar to the epinephrine-binding pocket of the beta-adrenergic receptor (BAR; Strader *et al.*, 1989; Freddolino *et al.*, 2004) and other ORs (Vaidehi *et al.*, 2002) and to 11*cis*-retinal pocket in bovine rhodopsin (Palczewski *et al.*, 2000). These figures show that the ligand binding pocket is located in between TM helices 3, 4 and 6. The residues making direct contact with the odorant are in the hypervariable region in the sequence alignment of ORs (Buck and Axel, 1991; Singer *et al.*, 1995a,b;

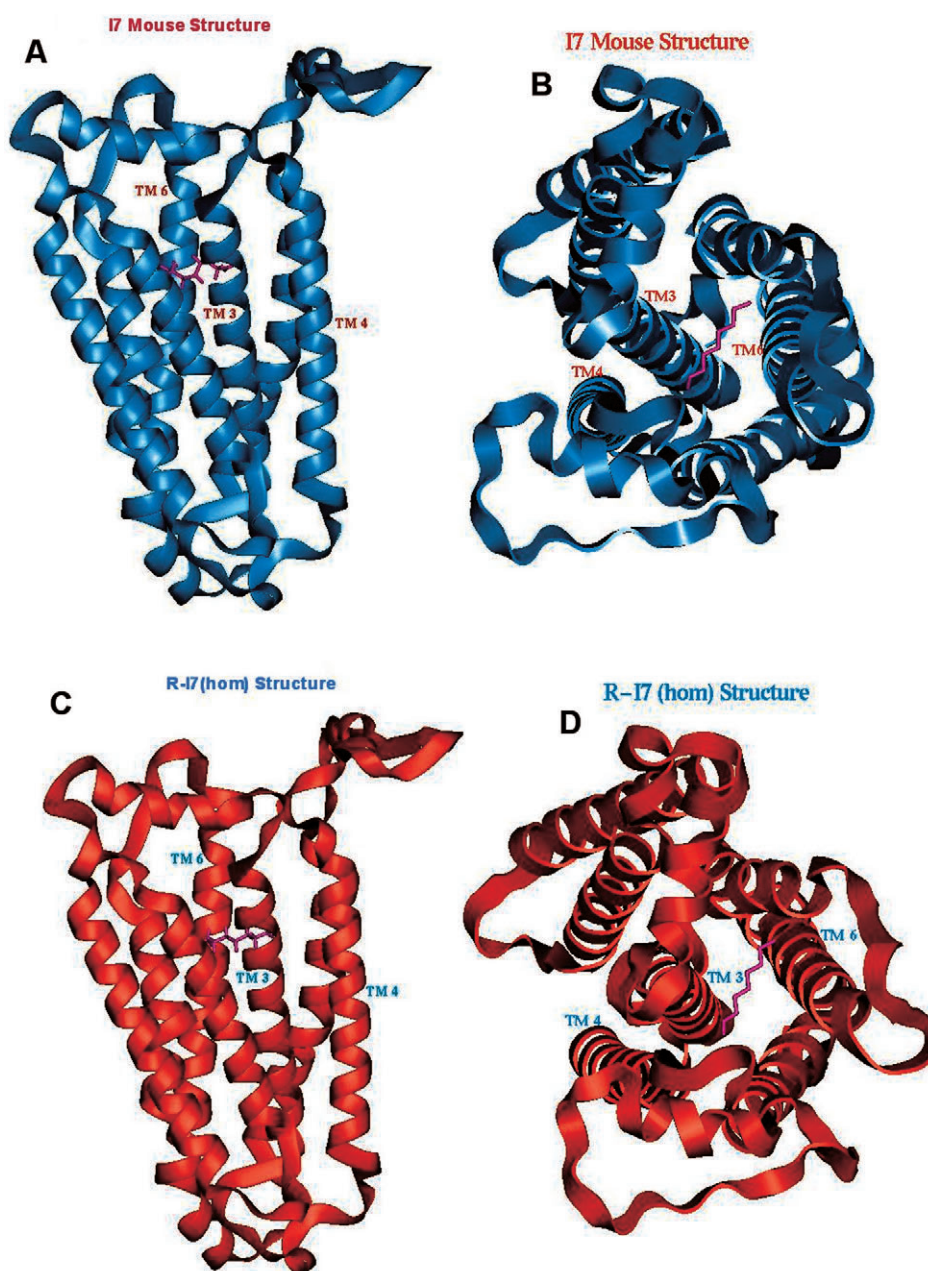


Figure 3 (A–D) Predicted 3-D structure for M-I7 OR and R-I7(hom) OR including the predicted binding location for octanal (purple). Transmembrane domains with residues involved in binding: 3, 4 and 6 are labeled. The disulfide bonds were assigned between Cys102–Cys184 and Cys174–Cys194.

Mombaerts, 1999; Pilpel and Lancet, 1999), consistent with their involvement in differential odor binding for different OR subtypes.

The details of the binding site of octanal in M-I7 and R-I7 structures are shown in Figure 4A,B, respectively. We find that Lys 164 is hydrogen bonded to the polar moiety for all the positive agonists, making it one of the critical residues for the binding of aldehydes. This could be directly tested experimentally by mutating this residue to uncharged polar residues (Tyr, Thr), which might switch receptor specificity toward odorants with polar but uncharged functional groups (say alcohols or ketones) or by mutating it to a nonpolar residue, which should lead to a dramatically different binding profile (or possibly to misfolding). Other residues that are involved in binding are: Ile 255, Ala 258, Ala 259, Ser 280 and Tyr 283. As detailed later in the text, mutating these residues might modulate the length of the alkyl chain recognized by these receptors. Tables 6 and 7 show the distances of the residues in the binding site of R-I7(hom) and M-I7 structures for the aldehydes predicted to be the best binders.

Description of binding sites of odorants with good binding energies

Citral, citronellal (+) and (-), heptanal, hexanal, nonanal and trans-cinnamaldehyde to M-I7. The binding site and orientation of citral, citronellal (+) and (-), heptanal, hexanal, nonanal and *trans*-cinnamaldehyde were all the same as octanal (Figure 4A). This is shown in Figure 4C for citral (yellow), nonanal (lime) and *trans*-cinnamaldehyde (orange). For each ligand, the long axis of the odorant is parallel to the membrane. In all these agonists the aldehyde functional group makes a hydrogen bond to Lys 164. The size of the odorant that can fit sufficiently near Lys 164 to hydrogen bond is modulated by Cys 114, Cys 117 and Phe 205. The length of the odorant binding in this mode is limited by the Ile 255, Ala 258, Ala 259, Ser 280 and Tyr 283. This suggests the residues that might be mutated to modify the binding profile and thereby validate our predictions.

Octanal, citral, citronellal (+) and (-), heptanal, hexanal, nonanal and trans-cinnamaldehyde to R-I7(hom). The predicted binding site of these eight ligands in R-I7(hom) (see Figure 4B) has the aldehyde functional group hydrogen bonded to Lys 164. The binding site near Lys 164 is shaped into a narrow groove lined by the residues: Cys 114, Cys 117, Phe 205 and Ile 209 which is very similar in R-I7(hom) and M-I7. Table 8 shows the differences in the binding pocket for the experimentally observed agonists and for decanal. The main difference between these two receptors is that Leu 110 is closer to the binding pocket in M-I7 while Phe 205 and Ile 209 are farther away from the binding pocket in M-I7. This may explain why citronellal binds more strongly to M-I7. The residues near Lys 164 form a groove that is narrower in R-I7(hom) than the corresponding groove in M-I7 and

the residues that limit the length of the ligand: Ile 255, Ala 258, Ala 259, Ser 280 and Tyr 283 are generally closer in R-I7(hom), which may explain why the longer ligand nonanal is experimentally observed in M-I7 and not in R-I7(hom). However, there is a report that nonanal is experimentally observed but with a weaker response (Araneda *et al.*, 2000). These distances differ just slightly for each ligand and the long axis of the odorant is again perpendicular to the membrane. Since our calculations indicate similar binding constants for these ligands, it could be that any differences observed experimentally might arise from other factors such as the ease of activation following binding of agonist which might be affected by residues remote from the active site.

Decanal to M-I7 and R-I7(hom). We find that decanal binds to a site in M-I7 and R-I7(hom) very similar to octanal; however, decanal must twist along its long axis (horizontal) in order to fit into the binding site. This is due to Ile 255, Ala 258, Ala 259, Ser 280 and Tyr 283 that hinder the length of this aldehyde (see Figure 4D for M-I7). The initial experimental results (Bozza *et al.*, 2002) did not find activation by decanal, but as discussed below, experiments done after the calculations show that it does lead to activation but is slower than heptanal in I7 mouse. Indeed, Araneda *et al.* (2000) also find that decanal activates I7 rat. The twisting of the molecule to fit the binding site could cause strain and could be the cause for the slow activation, which caused it to be missed as an agonist in the initial experiments.

Lilial to M-I7 and R-I7(hom). We predict that lilial binds strongly, but it was not found experimentally to be a positive agonist. Indeed the predicted binding site for lilial is quite different than for the observed agonists, being nearly vertical (see Figure 4E for M-I7). This vertical binding (parallel to the membrane) of this odorant is stabilized by the hydrophobic residues: Leu 106, Phe 109, Leu 110, Ile 168, Phe 205, Phe 262 and Ile 263. These residues form a hydrophobic tunnel that might act as a path for the aldehydes to enter into the binding pocket. In the bovine rhodopsin crystal structure, the extracellular loop II is closed down into the TM region with 11*cis*-retinal bound. With lilial bound in its vertical binding site, this loop cannot close in the same way, perhaps explaining why lilial does not activate the OR. This speculation that lilial may serve as a competitive antagonist was tested experimentally (see below) and found not to be the case.

Lylal to M-I7 and R-I7(hom). We predict that lylal binds strongly, but it was not found experimentally to be an agonist. Indeed the predicted binding configuration for lylal is quite different than the observed agonists. The binding site is similar to the M-I7 octanal site with the exception that the aldehyde functional group of lylal is hydrogen bonded to Ser 280 while the alcohol functional group at the other end is hydrogen bonded to Lys 164 (see Figure 4F). Although

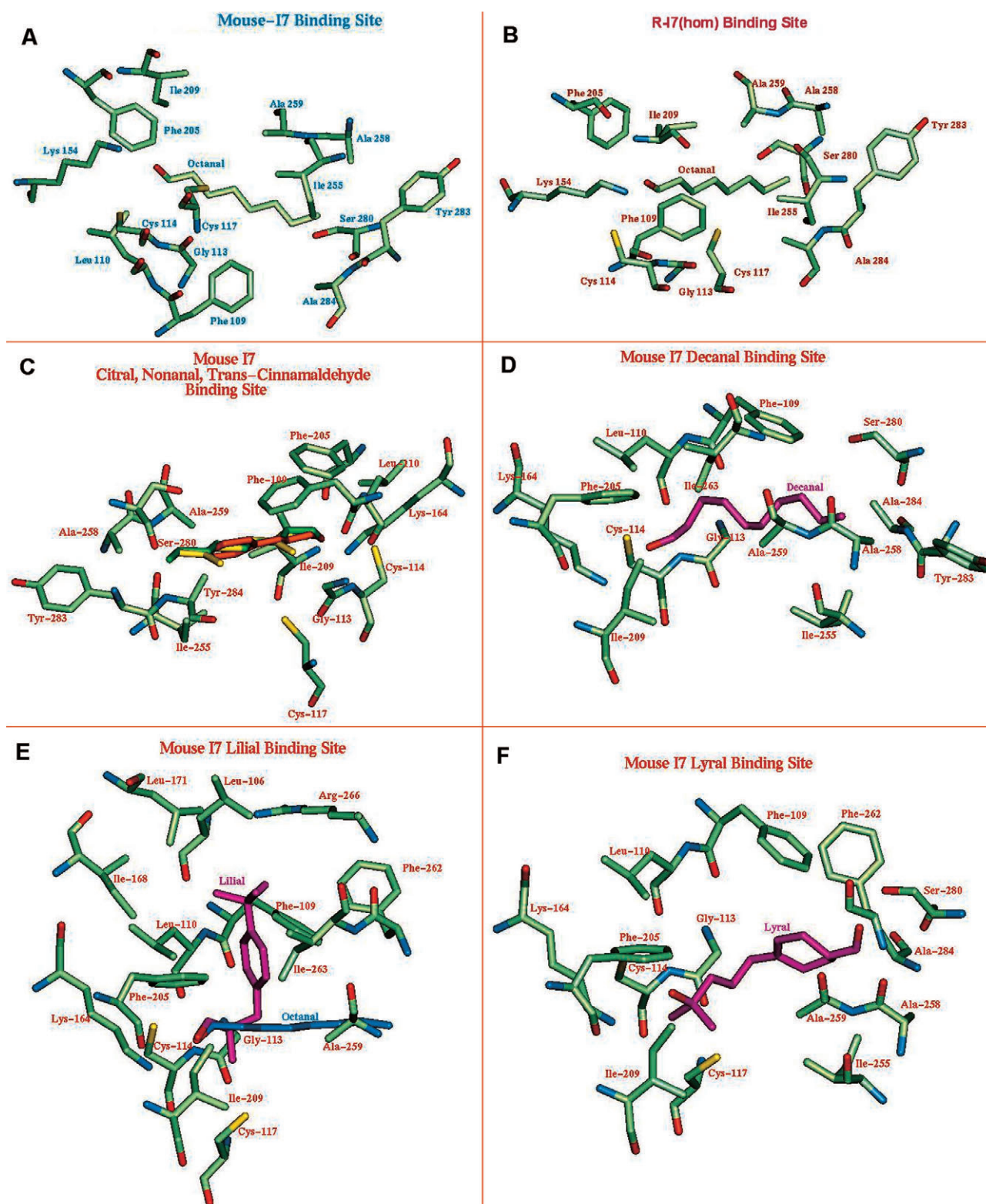


Figure 4 (A) Predicted recognition site for octanal in M-I7 OR (bottom view, looking up from the intracellular region). Residues within 3.5 Å of the ligand are displayed as thicker with labels in bold. Lys164 forms a hydrogen bond to the oxygen of the aldehyde. Transmembrane (TM) domains 3–7 have residues directly involved in binding. (B) Predicted recognition site for octanal in R-I7(hom) OR (bottom view). (C) Predicted recognition site for citral (yellow), nonanal (lime) and trans-cinnamaldehyde (orange) in M-I7 (side view, looking along a plane cutting the membrane region). (D) Predicted recognition site for decanal (purple) in M-I7 OR (side view). The twisting of the decanal in the binding pocket can be seen. (E) Predicted recognition site for lillal (purple) in M-I7 OR (side view). Octanal (blue) is used to show how lillal binds vertically in the protein. (F) Predicted recognition site for lylal (purple) in M-I7 OR (side view).

Table 6 For M-I7, we show the distance (Å) from the closest non-hydrogen side-chain atom in each residue to the closest non-hydrogen atom found in the final binding location of each of the ligands

Protein region	TM3						TM4		LP4	TM5		TM6					LP6	TM7		
A.A. sequence	L	F	L	G	C	C	K	I	L	F	I	I	A	A	F	I	R	S	Y	A
Res. No	106	109	110	113	114	117	164	168	171	205	209	255	258	259	262	263	266	280	283	284
Ligands																				
Citral		4.3	4.6	3.5	3.9	4.3	2.9			3.2	3.3	3.8	3.8	3.8				4.0	4.4	3.5
Citronellal (+)		4.2	4.1	3.9	3.6	3.5	2.9			3.4	3.7	3.8	3.9	3.8				4.0	4.4	3.5
Citronellal (–)		4.4	4.3	4.1	3.7	4.6	2.9			3.6	3.7	3.7	3.8	3.9				4.1	4.3	3.5
Decanal		3.5	4.0	4.5	3.7		2.9			3.2	3.7	4.0	3.4	3.8		5.3		3.8	4.6	4.5
Heptanal		4.8	4.2	4.6	3.6	4.5	2.9			3.5	3.8	4.0	5.0	3.8				4.2		4.0
Hexanal			4.2	4.6	3.6	4.5	2.9			3.5	3.8	4.3	5.1	3.8				4.9		5.4
Lilial	4.5	4.0	3.6	4.5	3.5	3.0	2.9	4.4	4.4	3.3	3.6			4.7	4.0	4.1	4.4			
Lylal		4.0	4.9	3.4	3.7	3.4	3.2			3.2	3.2	4.4	4.1	3.7	3.0			2.8		4.6
Nonanal		4.8	4.1	4.6	3.5	4.4	2.9			3.5	3.9	3.9	3.8	3.9				3.7	3.8	3.7
Octanal		4.8	4.2	4.5	3.6	4.5	2.9			3.5	3.8	3.8	3.8	3.8				4.0	4.2	4.1
Trans-cinnamaldehyde		4.5	4.2	4.5	3.7		2.9			3.4	3.8	3.5	4.6	3.4				4.8		5.2

The ligands shown are those that were experimentally positive or false positives. Those without numbers were too far to be in the binding pocket. Those residues that are hydrogen bonded to the odorant have their distances shown in bold.

Table 7 For R-I7(hom) we show the distance (Å) from the closest non-hydrogen side-chain atom in each residue to the closest non-hydrogen atom found in the final binding location of each of the ligands

Protein region	TM3						TM4		TM5		TM6				TM7		
A.A. sequence	F	L	G	C	C		K		F	I	I	A	A		S	Y	A
Res. No.	109	110	113	114	117		164		205	209	255	258	259		280	283	284
Ligands																	
Citral	4.3		5.0	3.6	3.9	4.6	2.9		3.3	3.4	3.8	3.7	3.8		4.0	4.4	3.5
Citronellal (+)	4.0			3.7	3.7	3.5	2.9		3.3	3.6	3.8	3.8	3.7		3.9	4.4	3.5
Citronellal (–)	4.2		4.2	4.4	3.7	4.5	2.9		3.3	3.6	3.8	3.8	3.9		4.0	4.3	3.4
Decanal	3.7		4.0	4.2	3.8	4.7	2.9		3.1	3.6	3.9	3.8	4.0		3.9	4.7	4.5
Heptanal	4.7			4.5	3.6	4.5	2.9		3.4	3.8	4.0		3.8		4.1		4.0
Hexanal	4.9			4.5	3.6	4.5	2.9		3.4	3.8	4.4	5.1	3.8		4.9		5.4
Nonanal	4.8			4.5	3.6	4.5	2.9		3.2	3.8	3.9	3.7	3.9		3.7	3.8	3.7
Octanal	4.8			4.5	3.6	4.5	2.9		3.3	3.8	3.8	3.7	3.8		4.0	4.2	4.0
Trans-cinnamaldehyde	4.4			4.3	3.7		2.9		3.4	3.7	3.6	4.7	3.6				4.9

The ligands shown are those that were experimentally positive or false positives. Those without numbers were too far to be in the binding pocket. Those residues that are hydrogen bonded to the odorant show their distances in bold.

this reversed binding site leads to a good predicted binding energy, its reversed orientation may be responsible for its inability as a positive agonist. This may indicate that strong binding to Lys 164 is necessary for activation. Thus lylal may serve as a competitive antagonist.

Summary of binding studies. To summarize the results on binding studies, we used HierDock to predict the most probable binding site of octanal for the M-I7 and R-I7(hom) structures and to predict the binding of all 62 odorants to this binding site. The corresponding binding energies are

Table 8 Shown are the differences in each distance from Table 7 minus the corresponding distance from Table 6 [i.e. comparison of R-I7(hom) and M-I7 binding pockets]

Protein region	TM3					TM4	TM5		TM6			TM7		
A.A. sequence	F	L	G	C	C	K	F	I	I	A	A	S	Y	A
Res. No.	109	110	113	114	117	164	205	209	255	258	259	280	283	284
Ligands														
Citral	0	0.4	0.1	-0.1	0.3	0	0.2	0	0	-0.1	0	0	0	0
Citronellal (+)	-0.2	M	-0.2	0.1	0.1	0	-0.1	-0.1	0	-0.1	-0.1	0	0	0
Citronellal (-)	-0.1	-0.1	0.3	0	-0.1	0	-0.3	-0.1	0	0	0	0	0	0
Decanal	0.2	0	-0.3	0.1	R	0	-0.1	-0.2	-0.1	0.3	0.2	0	0.1	0
Heptanal	0	M	-0.1	0	0	0	-0.2	-0.1	0	M	0	-0.1	0	0
Hexanal	R	M	-0.1	0	0	0	-0.1	-0.1	0	0	0	0	0	0
Nonanal	0	M	-0.1	0.1	0	0	-0.3	-0.1	0	0	0	0	0	0
Octanal	0	M	-0.1	0	0	0	-0.2	-0.1	0	0	0	0	0	0
Trans-cinnamaldehyde	0	M	-0.2	0	0	0	0.1	0	0.1	0.1	0.2	M	0	-0.3

The negative numbers represent the residues that are closer to the ligand in R-I7(hom) than to M-I7. The positive numbers in represent the residues that are closer to the ligand in M-I7 than to R-I7(hom). The letter 'M' represents a residue that is within 3.5 Å of the ligand in the M-I7 structure but not in the R-I7(hom) and the letter 'R' represents a residue that is within 3.5 Å of the ligand in R-I7(hom) but not in M-I7. The distance 3.5 Å is used to filter out all non-significant interactions in the binding pocket.

shown in Table 5, where we find a good comparison with the experiments. Again both M-I7 and R-I7 are predicted to bind both heptanal and octanal. As discussed above, some of the experiments in literature had indicated that heptanal activates M-I7 but not R-I7 while octanal activates R-I7 but not M-I7 (Krautwurst *et al.*, 1998), but later experiments (Bozza *et al.*, 2002) find that both lead to activation. The calculated binding energies also agree with literature that nonanal and decanal activate I7 rat (Araneda *et al.*, 2000; Levasseur *et al.*, 2003). Lys164 forms a hydrogen bond with the aldehyde group of the aldehyde agonists, This was also previously observed by Singer (2000).

Agonists, antagonists, binding of mixtures

A difficulty in comparing the calculated binding energies directly to the experimental activation data is that a strongly bound odorant could be an agonist (eliciting intracellular calcium ion influx) or an antagonist (preventing activation of the OR). However, most experiments on ORs detect only agonists. Consequently, we are particularly concerned about comparing the calculated binding energies of odorants to experiments done only on mixtures, since a mixture containing an antagonist might mask the activation by an agonist (Cromarty and Derby, 1998). There could also be cases where two ligands both interact with the same receptor, which is outside the scope of our current studies. Antagonists could be sought experimentally by competitive binding studies of suspected antagonists against known agonists. This might identify OR inhibitors that could impair the detection of specific odorants. We have compared

the predicted binding energies only to the experimental agonists that have been tested as individual odorants. For cases in which only mixtures were known to not elicit activation of the ORs, we did not assume that the single components are non-binders.

Proposed competitive experiments and verification

Based on the first generation of predicted structures (pre-RI7 and pre-MI7) for rat and mouse I7, we predicted three ligands: decanal, lyral and lilial to have good binding energies (within the top 10%) which were not observed agonists to these ORs. Since cinnamaldehyde (an observed agonist) was predicted to bind in a similar location and structure as lilial and lyral and with a similar binding energy, we speculated that lilial and lyral might be antagonists. Similarly heptanal (an observed agonist) is predicted to bind in location and structure similar to decanal and with a similar binding energy, but again decanal did not elicit activation response. At that stage, we proposed three experiments that could be done to test for competitive binding to M-I7: (i) cinnamaldehyde versus lilial; (ii) cinnamaldehyde versus lyral; and (iii) decanal versus heptanal.

Competitive activation assays for decanal and lilial

The proposed competitive experiments were carried out to test the above suggestions (Bozza, personal communication). Specifically, Bozza tested whether decanal or lilial can inhibit responses to the known I7 agonists heptanal or cinnamaldehyde, respectively.

In the new experiments on decanal using a variety of concentrations, it was found to be an agonist but slower than heptanal or cinnamaldehyde. Concentration of the ligand can affect the binding affinity (Levasseur *et al.*, 2003) and thus suggesting that nonanal and decanal are weaker agonists to I7 rat (Araneda *et al.*, 2000).

However, the experimental results showed that linal does not behave as a robust inhibitor of cinnamaldehyde for mouse I7 OR (Bozza, personal communication). Thus the predicted binding of linal must be assumed to be a false positive, while experiments show that decanal does activate the receptor, as predicted by the theory.

Filtering false positives with moments of inertia

Since the competitive experiments suggested that linal neither agonizes nor antagonizes I7, we suspected that there might be a size restriction on which ligands could bind and activate the I7 mouse OR, as also discussed in Araneda *et al.* (2000). Such a restriction might result from difficulties in the odorant successfully diffusing into the binding site. To test this idea we calculated the moments of inertia for the final bound structures of all the aldehydes to the M-I7 model (see Table 9). The moments of inertia were calculated by assigning each atom with its atomic weight and then finding the axis that correspond to the highest distribution of the mass of the ligand. These numbers represent the general size of the ligand, since the larger the number the farther away

from the axis the density is. Since the agonists all have a small first moments of inertia number, this means that the binding site prefers a long narrow shape opposed to a rounder or fatter one. This correlates well with the observations that molecular length is critical for rat I7 that are found in Araneda *et al.* (2000). This first small moments of inertia component is aligned with the long axis of the ligand. We found that the two smaller moments of inertia for linal and lylal are larger than those for the odorants compounds observed to be agonists to M-I7. Indeed, Figure 5 shows that comparing these two moments with the binding energy scores leads to a contour map (Figure 5) in which all false positives are well separated from the true positives for the M-I7 profile.

Based on these results we defined the new scoring function in equation (1) that combines these two moments of inertia with the docking energy score. This equation was developed to fit the preferred moments of inertia trend observed in Figure 5. Those ligands observed to be in the right shape (by moments of inertia) were weighted to keep most of their original energy scores, while those that are farther from the right shape are given increasingly larger penalties to the original energy score. Sorting the aldehydes with this new weighted score puts all the observed agonists at the top (Table 9), plus it suggests that decanal is a weaker agonist. This provides an empirical relation that can be used to testing for new agonists.

Table 9 The principle moments of inertia for the final bound structure of each aldehyde in the M-I7 structure

Aldehydes	Moments of inertia			Binding energy	Weighted energy score
	1st	2nd	3rd		
Citronellal (+)	153.1	1727.4	1837.8	36.3917	36.2
Citronellal (–)	152.7	1746.8	1828.2	35.349	35.2
Octanal	50.8	1486.1	1508.3	34.6702	34.1
Heptanal	43.6	1045	1063.4	32.0736	31.2
<i>Trans</i> -cinnamaldehyde	110.4	878.7	989.1	29.5612	29.1
Decanal	191.2	1606.3	1651.2	29.2197	28.6
Citral	153.5	1717	1840.8	27.9483	27.8
Hexanal	37.9	692.9	708.6	29.6216	26.8
Nonanal	57.1	2048	2072.1	28.3484	26.4
Valeraldehyde	31.2	434	446.4	27.2348	19.7
Benzaldehyde	102.4	329.1	431.5	25.7413	16.5
Butyraldehyde	24.6	246.7	255.9	25.1915	10.7
Ethylvanillin	307.4	884.2	1106.7	25.6546	–4.9
Lilial	383.3	2066.6	2111.2	33.1472	–86.0
Lylal	439.9	2397.6	2564.5	31.4951	–232.6

Those aldehydes whose names are shaded are positive agonists as found experimentally (Bozza *et al.*, 2002). The aldehydes are sorted by the weighted energy score from equation (2). Note that subsequent experiments (Bozza, personal communication) found that decanal also binds experimentally.

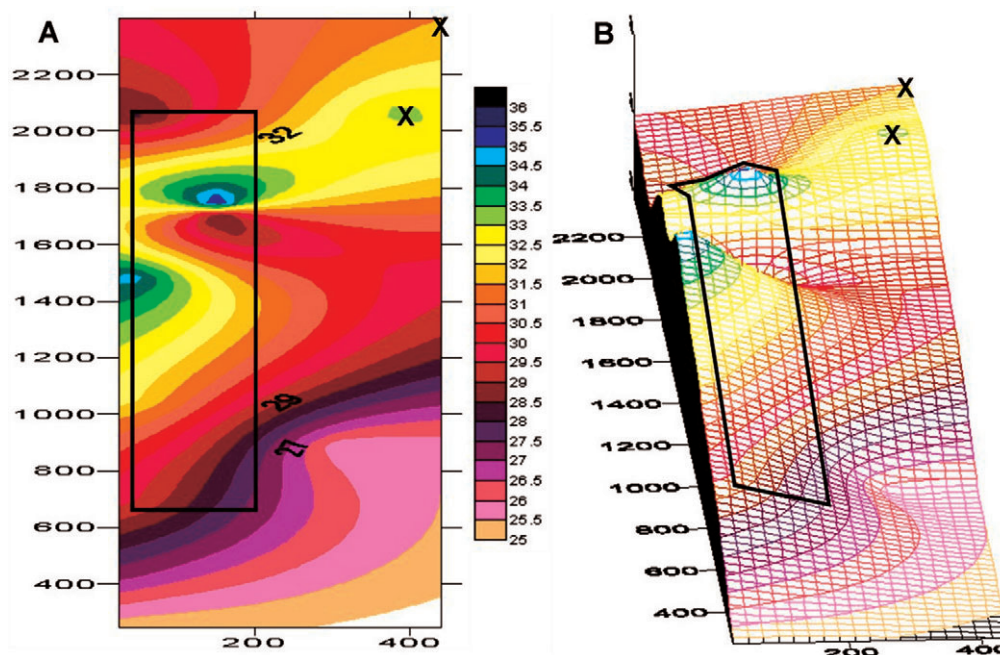


Figure 5 (A, B) This figure consists of (A) a contour map and (B) a wireframe map of the binding energy versus the two smaller moments of inertia from the data in Table 8. The two smaller moments of inertia are the x - and y -axes and the binding energy is the z -axis. The positive agonists tend to have I_x (first moment) between 36 and 200 and I_y (second moment) = 650–2050. This is shown as a rectangle. In contrast the false positives lylal and lilial have I_x , I_y = 439.9, 2397.6 and 383.3, 2066.6, respectively. This is shown as two large crosses.

$$a = b - \left(\frac{c_1 - 120}{80} \right)^4 - \left(\frac{c_2 - 1375}{600} \right)^4 \quad (1)$$

where a is the weighted energy score, b is the bonding energy score, and c_1 and c_2 are the first and second moments of inertia respectively.

After determining that this expression works for aldehydes, we applied it to the other molecules in the odorant library for both mouse and rat I7 (see Table 10). We found a good correlation to experimental activation measurements (now including decanal as a positive agonist for mouse I7). Thus we find that 100% of class A (eight compounds), 90% (including the literature results for decanal and nonanal for I7 rat) of class B (10 compounds) and none of the poor binder classes were observed (106 compounds) to be agonists. Of course, the use of such an empirical relation to predict the agonists is not fully satisfactory. Thus we will continue to search for improved atomistic methods that predict correctly the ligands that activate these receptors without the use of empirical data.

Discussion

The correlation between the calculated binding energies and the measured experimental calcium ion influx suggests that the combination of experimental functional assays with OR structure prediction will make it possible to identify potential odors for other ORs. Even more important the knowledge of the detailed binding site suggests site-directed mutations experiments that would validate the predictions. Indeed the theory could be used to determine mutations that

would increase the selectivity for particular odorants or even to modify the ORs to be selective against new odorants. Theoretical predictions provide an atomic level understanding of the odorant binding to ORs. This might be used to enhance the development of biosensors for the fragrance and food industries, industrial and environmental safety and explosives and narcotics detection.

Additional experiments to directly test the predictions made here would be most useful. Such comparisons could help develop knowledge based methods to predict the function of GPCRs in terms of pharmacophore models that might accelerate the predictions of the response patterns of new odorants.

Proposed experiments

The in-depth analysis of the dimensions of the binding site of odorants in the final structure of M-I7 discussed above shows that Lys 164, Cys 117 and Ser 280 are main contributors to ligand binding. Indeed, the Lys 164 might well play an essential role beyond the binding mode we have studied. We suggest that Lys 164 might form a Schiff's base with the aldehyde agonists just as is known to occur with 11*cis*-retinal in bovine rhodopsin. Thus the first step of noncovalent binding which we find to strongly prefer aldehyde, might position the aldehyde for a subsequent formation of the Schiff's base, which could be responsible for the changes in conformation that lead to activation. If such chemical events play a special role in activation, it could have a significant impact on how we think about the binding in ORs and

Table 10 Calculated moment-weighted energy score from equation (2) for the 62 odorants docked to M-I7 and R-I7(hom) (MembStruk 2.0)

Main functional group	M-I7		R-I7 (hom)	
	Odorants	M. of inert. energy	M. of inert. Energy	Odorants
Alcohols	Octanol	18.048	17.757	2-Phenylethanol
	Geraniol	14.862	16.861	Octanol
	1-Decanol	11.474	14.015	Geraniol
	Hexanol	11.358	12.636	Hexanol
	2-Phenylethanol	10.972	8.433	Linalool (+)
	Eugenol	6.903	5.982	1-Decanol
	Isopulegol	4.928	2.941	Isopulegol
	Butanol	-3.023	-4.332	Butanol
	Linalool (+)	-19.671	-25.944	Linalool (-)
	Linalool (-)	-27.325	-106.587	Eugenol
Aldehydes	Citronellal (+)	36.243	37.469	Citronellal (+)
	Citronellal (-)	35.174	33.859	Octanal
	Octanal	34.109	32.710	Citronellal (-)
	Heptanal	31.150	30.958	Heptanal
	Trans-cinnamaldehyde	29.093	29.937	Decanal
	Decanal	28.570	28.867	Citral
	Citral	27.812	28.414	Trans-cinnamaldehyde
	Hexanal	26.842	26.562	Hexanal
	Nonanal	26.383	26.101	Nonanal
	Valeraldehyde	19.667	19.163	Valeraldehyde
	Benzaldehyde	16.506	17.345	Benzaldehyde
	Butyraldehyde	10.664	9.971	Butyraldehyde
	Ethylvanillin	-12.579	-17.224	Lilial
	Lilial	-85.957	-114.238	Ethylvanillin
	Lylal	-232.623	-1042.625	Lylal
Amine	Phenethylamine	14.023	14.178	Phenethylamine
Carboxylic acids	Octanoic acid	-48.890	-45.371	Octanoic acid
	Hexanoic acid	-57.139	-51.719	Hexanoic acid
	Butyric acid	-62.958	-65.235	Butyric acid
	Propionic acid	-74.896	-75.955	Propionic acid
	Decanoic acid	-160.470	-155.570	Decanoic acid
Esters	Hexyl acetate	21.736	21.123	Estragole
	Estragole	21.089	15.932	Benzyl propionate
	Ethyl benzoate	16.680	15.767	Ethyl benzoate
	Benzyl propionate	13.487	13.966	Hexyl acetate
	n-Butyl acetate	13.068	13.007	Propyl butyrate
	Propyl butyrate	9.418	11.330	n-Butyl acetate
	Ethyl acetate	3.217	0.781	Ethyl acetate

Experimentally obs.

Exper. not tested

Table 10 Continued

Main functional group	M-I7		R-I7 (hom)	
	Odorants	M. of inert. energy	M. of inert. Energy	Odorants
Esters	Amyl butyrate	-139.888	-196.184	Amyl butyrate
	Octyl acetate	-206.834	-342.117	Allyl phenoxyacetate
	Heptyl butyrate	-372.001	-463.098	Heptyl butyrate
	Allyl phenoxyacetate	-429.140	-888.139	Octyl acetate
Ether	Eucalyptol	-58.750	-57.817	Eucalyptol
Ketones	S-pos-carvone	20.287	20.542	S-pos-carvone
	Butyrophenone	18.106	16.806	Ethylisoamylketone
	R-neg-carvone	17.056	16.085	2-Aminoacetophenone
	2-Octanone	14.014	13.921	Butyrophenone
	Propiophenone	13.516	13.624	Propiophenone
	Ethylisoamylketone	13.203	9.922	Acetophenone
	2-4-Dimethylacetophenone	10.202	9.603	2-4-Dimethylacetophenone
	Acetophenone	10.097	9.513	R-neg-carvone
	Menthone_1	9.275	8.480	Menthone_1
	2-Aminoacetophenone	8.944	8.119	2-Hexanone
	2-Hexanone	8.516	4.593	Menthone_4
	Menthone_4	6.107	1.495	2-Octanone
	Menthone_2	-3.776	-4.140	Menthone_3
	2-Butanone	-8.996	-5.800	Menthone_2
	Menthone_3	-25.383	-6.783	2-Butanone
	2-Sec-butylcyclohexanone	-48.113	-20.786	Valerophenone
	Valerophenone	-119.943	-45.283	2-Sec-butylcyclohexanone
	Beta-ionone	-419.200	-372.824	Beta-ionone
	Hedione	-6582.995	-716.726	Hedione

Those ligand names that experimentally tested positive for being an antagonist are shaded. Note that subsequent experiments (Bozza, personal communication) found that decanal also binds experimentally to M-I7 and from the literature decanal and nonanal bind to I7 rat.

we strongly suggest experimental tests of these highly speculative suggestions. For example, mutating Lys164 to such polar groups as Arg or His might still bind an aldehyde but would not form a Schiff base. Similarly mutation to Asn or Gln or even Ser, Thr, or Tyr might still bind an aldehyde but would not accommodate the covalent attachment. This might explain the preference of I7 towards aldehydes.

Lys 164, Cys 117 and Ser 280 along with Phe 205 and Phe 109 cap the width of the binding pocket, forming a pocket that is ~8 Å long and ~4 Å deep (see Figure 6). Using this predicted binding pocket, we now consider the design of novel odor agonists that should bind strongly to the mouse I7 receptor and may lead to activation. We considered several multi-functional potential ligands, which we subjected to the HierDock2.0 protocol. The best of these

suggested potential odorants (8-hydroxy-octanal) has two chemical functional groups, with character very different than the known agonists for I7. 8-hydroxy-octanal has the following strong interactions with I7: Lys 164 to the aldehyde functional group and Ser 280 to the alcohol group. Thus experiments on the binding of this compound would serve as a good test on the value of the theory to predict binding and activity.

Summary and conclusions

We have used MembStruk2.0 and HierDock2.0 methods to predict the structures and odorant binding sites of 56 odorants in two closely related ORs: mouse and rat I7. The predicted binding site of odorants is located in TM domains

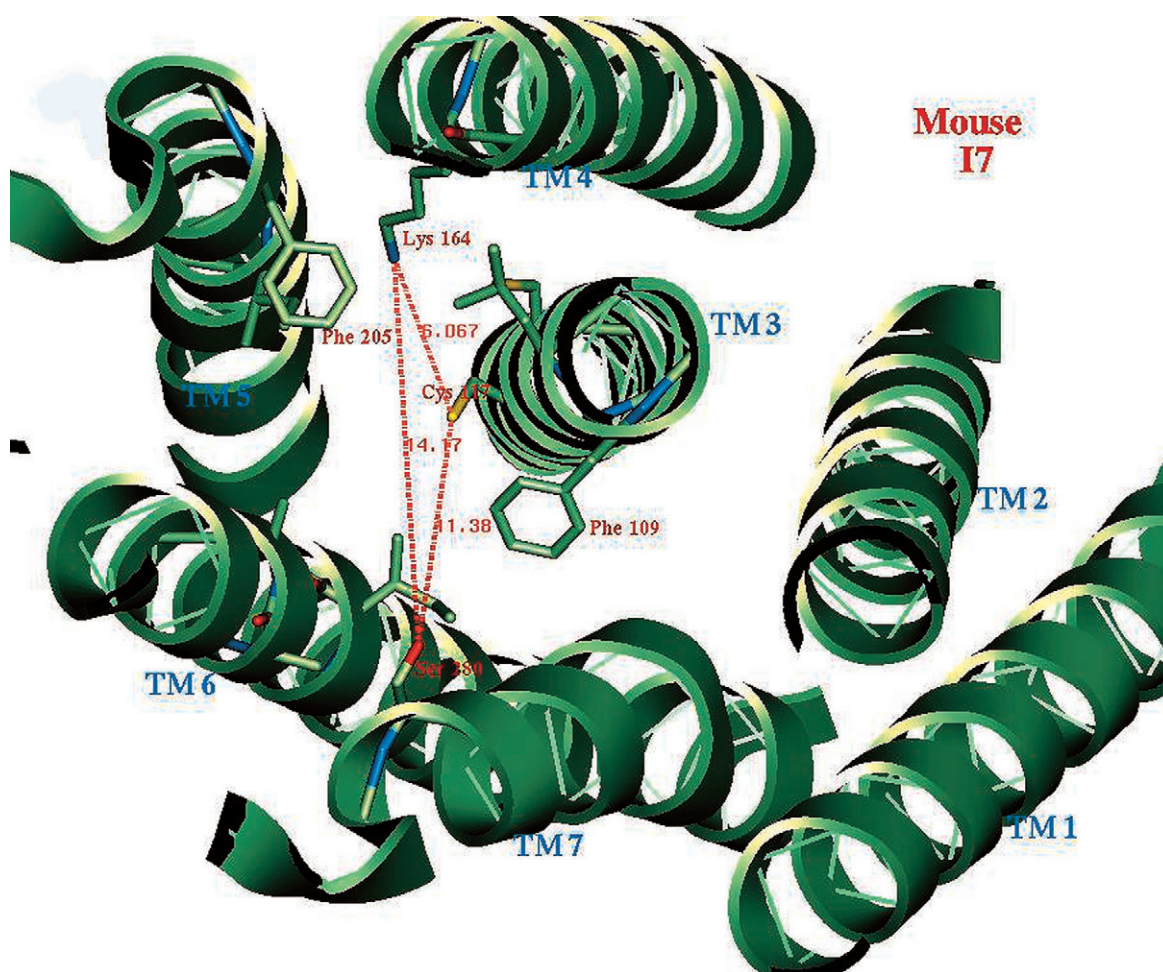


Figure 6 Binding pocket of odorants in M-I7, top view (looking down from the extracellular region). The three residues (Cys 117, Lys 164, Ser 280) that can form possible hydrogen bonds to a ligand are shown with their distances. Also shown are residues 205 and 109 that limit the width of the binding pocket. This pharmacophore model has been used to derive new odorants that can be potential agonists for M-I7 receptor. These are described briefly in the text.

3, 4 and 6. In particular Lys164, Phe109, Cys114, Cys117 and Ile255 of TM4 are predicted to be involved in recognition of octanal and other aldehydes in the I7 receptor. This suggests that mutation experiments could be used to test further our predictions. Thus the mutation of Lys164 should dramatically change the recognition profile of M-I7 and R-I7.

The calculated binding energy of octanal and heptanal to both M-I7 and R-I7 are nearly equal and hence we predicted that both heptanal and octanal would activate the receptors. This was subsequently confirmed by experimental measurements on the intracellular calcium concentration influx. Also out of the top 10% of the calculated best binding odorants, 62% were observed to be agonists experimentally and out of the next 15% in the binding energy list, 33% were observed to be agonists. None of the bottom 75% of the worst binders was observed to be agonist. This provides an overall validation of the predicted structures for these proteins and of the methods.

The results presented here demonstrate significant progress toward predicting structure and function of olfactory receptors (and other GPCRs). Each of these predictions can be directly tested experimentally. Development of the atomistic structural models for ORs with specific binding requirements for specific odorants to provide information that could be valuable in making the connection between binding, processing to the cortex, to eventually perception and psychological response. Understanding these relationships could have significant impact on the fragrance and food industries and might be useful in developing artificial olfaction sensors.

Indeed as the accuracy of the predicted OR structures are validated, it should be practical and useful to predict the 3-D structures of all 913 mouse ORs and all 339 human ORs. Then it would be practical to predict the binding of large odorant libraries to all olfactory receptors to obtain overall binding profiles that could be most useful in tracing through

the processing connecting molecular recognition to odorant recognition.

Supplementary material

Supplementary material can be found at: <http://www.chemse.oupjournals.org/>

Acknowledgements

We thank Dr Thomas Bozza and Professor Peter Mombaerts of Rockefeller University for their suggestion of the blind test on I7 and their assistance in this collaboration. Our special thanks to Dr Thomas Bozza for conducting some competitive assay experiments proposed by us. This work was initiated with support by ARO-MURI (Dr Robert Campbell) with some of the HierDock work supported by NIH (BRGRO1 and GM625523). The computational facilities used here were supported by an IBM-SUR grant and by an ARO-DURIP grant. Other facilities of the Materials and Process Simulation Center used in this project are supported also by DOE (ASCI ASAP), General Motors, ChevronTexaco, ONR, NSF (CHE and MRI), ARO, ONR, Beckman Institute, Seiko-Epson, NIH HD and Asahi Kasei.

References

- Araneda, R.C., Kini, A.D. and Firestein, S. (2000) *The molecular receptive range of an odorant receptor*. Nat. Neurosci., 3, 1248–1255.
- Araneda, R.C., Mermet, N., Verjat, T., Angulo, J.F. and Radicella, J.P. (2001) *Expression of Kin17 and 8-OxoG DNA glycosylase in cells of rodent and quail central nervous system*. Brain Res. Bull., 56, 139–146.
- Bower, M., Cohen, F.E. and Dunbrack, R.L., Jr (1997) *Prediction of protein side-chain rotamers from a backbone-dependent rotamer library: a new homology modeling tool*. J. Mol. Biol., 267, 1268–1282.
- Bozza, T. and Kauer, J.S. (1998) *Odorant response properties of convergent olfactory receptor neurons*. J. Neurosci., 18, 4560–4569.
- Bozza, T., Feinstein, P., Zheng, C. and Mombaerts, P. (2002) *Odorant receptor expression defines functional units in the mouse olfactory system*. J. Neurosci., 22, 3033–3043.
- Buck, L. and Axel, R. (1991) *A novel multigene family may encode odorant receptors: a molecular basis for odor recognition*. Cell, 65, 175–187.
- Connolly, M.L. (1983) *Solvent-accessible surfaces of proteins and nucleic acids*. Science, 221, 709–713.
- Cromarty, S.I. and Derby, C.D. (1998) *Inhibitory receptor binding events among the components of complex mixtures contribute to mixture suppression in responses of olfactory receptor neurons of spiny lobsters*. J. Comp. Physiol. A, 183, 699–707.
- Ding, H.Q., Karasawa, N. and Goddard, W.A., III (1992a) *Atomic level simulations on a million particles: the cell multipole method for Coulomb and London nonbond interactions*. J. Chem. Phys., 97, 4309–4315.
- Ding, H.Q., Karasawa, N. and Goddard, W.A., III (1992b) *Atomic level simulations on a million particles: the cell multipole method for Coulomb and London nonbond interactions*. Chem. Phys. Lett., 196, 6–10.
- Donnelly, D. (1993) *Modelling alpha-helical transmembrane domains*. Biochem. Soc. Trans., 21, 36–39.
- Duchamp-Viret, P., Chaput, M.A. and Duchamp, A. (1999) *Odor response properties of rat olfactory receptor neurons*. Science, 284, 2171–2174.
- Eisenberg D., Weiss R.M. and Terwilliger, T.C. (1984) *The hydrophobic moment detects periodicity in protein hydrophobicity*. Proc. Natl Acad. Sci. USA, 8, 140–144.
- Ewing, T.A. and Kuntz, I.D. (1997) *Critical evaluation of search algorithms for automated molecular docking and database screening*. J. Comput. Chem., 18, 1175–1189.
- Filizola, M., Perez, J.J. and Carteni-Farine, M. (1998) *BUNDLE: a program for building the transmembrane domains of G-protein-coupled receptors*. J. Comput. Aided Mol. Des., 12, 111–118.
- Floriano, W.B., Vaidehi, N., Singer, M.S., Shepherd, G.M. and Goddard, W.A., III (2000) *Molecular mechanisms underlying differential odor responses of a mouse olfactory receptor*. Proc. Natl Acad. Sci. USA, 97, 10712–10716.
- Freddolino, P.L., Kalani, M.Y., Vaidehi, N., Floriano, W.B., Hall, S.E., Trabanino, R.J., Kam, V. and Goddard, W.A., III (2004) *3-D structure for human b2 adrenergic receptor and the binding site for agonists and antagonist*. Proc. Natl Acad. Sci. USA, 101, 2736–2741.
- Gasteiger, J. and Marsili, M. (1980) *Iterative partial equalization of orbital electronegativity—a rapid access to atomic charges*. Tetrahedron, 36, 3219–3228.
- Ghosh, A., Rapp, C.S. and Friesner, R.A. (1998) *Generalized Born model based on a surface integral formulation*. J. Phys. Chem. B, 102, 10983–10990.
- Godfrey, P.A., Malnic, B. and Buck, L.B. (2004) *The mouse olfactory receptor gene family*. Proc. Natl Acad. Sci. USA, 101, 2156–2161.
- Grigorieff, N., Ceska, T.A., Downing, K.H., Baldwin, J.M. and Henderson, R. (1996) *Electron-crystallographic refinement of the structure of bacteriorhodopsin*. J. Mol. Biol., 259, 393–421.
- Jain, A., Vaidehi, N. and Rodriguez, G. (1993) *A fast recursive algorithm for molecular dynamics simulation*. J. Comp. Phys., 106, 258–268.
- Kajiya, K., Inaki, K., Tanaka, M., Haga, T., Kataoka, H. and Touhara, K. (2001) *Molecular bases of odor discrimination: reconstitution of olfactory receptors that recognize overlapping sets of odorants*. J. Neurosci., 21, 6018–6025.
- Kalani, M.Y., Vaidehi, N., Freddolino P.E., Floriano W.B., Hall, S.E., Trabanino, R.J., Kam V. and Goddard, W.A., III (2004) *Structure and function of human D_{2L} receptor*. Proc. Natl Acad. Sci. USA, 101, 3815–3820.
- Kiefer, H., Krieger, J., Olszewski, J.D., von Heijne, G., Prestwich, G.D. and Breer, H. (1996) *Expression of an olfactory receptor in Escherichia coli: purification, reconstitution and ligand binding*. Biochemistry, 35, 16077–16084.
- Krautwurst, D., Yau, K.W. and Reed, R.R. (1998) *Identification of ligands for olfactory receptors by functional expression of a receptor library*. Cell, 95, 917–926.
- Lancet, D., Sadovsky, E. and Seidemann, E. (1993) *Probability model for molecular recognition in biological receptor repertoires: significance to the olfactory system*. Proc. Natl Acad. Sci. USA, 90, 3715–3719.
- Levasseur, G., Persuy, M., Grebert, D., Remy, J., Salesse, R. and Pajot-Augy, E. (2003) *Ligand-specific dose-response of heterologously expressed olfactory receptors*. Eur. J. Biochem., 270, 2905–2912.
- Lim, K.-T., Brunett, S., Iotov, M., McClurg, R.B., Vaidehi, N., Dasgupta, S., Taylor, S. and Goddard, W.A., III (1997) *Molecular dynamics for very large systems on massively parallel computers: the MPSim program*. J. Comput. Chem., 18, 501–521.
- Malnic, B., Hirono, J., Sato, T. and Buck, L.B. (1999) *Combinatorial receptor codes for odors*. Cell, 96, 713–723.

- Malnic, B., Godfrey, P.A. and Buck, L.B.** (2004) *The human olfactory receptor gene family*. *Proc. Natl Acad. Sci. USA*, 101, 2584–2589.
- Mathiowetz, A.M., Jain, A., Karasawa, N. and Goddard, W.A., III** (1994) *Protein simulations using techniques suitable for very large systems: the cell multipole method for nonbond interactions and the Newton–Euler inverse mass operator method for internal coordinate dynamics*. *Proteins*, 20, 227.
- Mayo, S.L., Olafson, B.D. and Goddard, W.A., III** (1990) *DREIDING: a generic force field for molecular simulations*. *J. Phys. Chem.*, 94, 8897–8909.
- Mombaerts, P.** (1999) *Seven-transmembrane proteins as odorant and chemosensory receptors*. *Science*, 286, 707–711.
- Mori, K., Nagao, H. and Yoshihara, Y.** (1999) *The olfactory bulb: coding and processing of odor molecule information*. *Science*, 286, 711–715.
- Palczewski, K., Kumasaka, T., Hori, T., Behnke, C., Motoshima, H., Fox, B., Trong, I., Teller, D., Okada, T., Stenkamp, R., Yamamoto, M. and Miyano, M.** (2000) *Crystal structure of rhodopsin: a G-protein-coupled receptor*. *Science*, 289, 739–745.
- Pilpel, Y. and Lancet, D.** (1999) *The variable and conserved interfaces of modeled olfactory receptor proteins*. *Protein Sci.*, 8, 969–977.
- Poincelot, R.P., Millar, P.G., Kimbel, R.L. Jr and Abrahamson, E.W.** (1970) *Determination of the chromophoric binding site in native bovine rhodopsin*. *Biochemistry*, 9, 1809–1816.
- Rappé, A.K. and Goddard, W.A., III** (1991) *Charge equilibration for molecular dynamics simulations*. *J. Phys. Chem.*, 95, 3358.
- Rubin, B.D. and Katz, L.C.** (1999) *Optical imaging of odorant representations in the mammalian olfactory bulb*. *Neuron*, 23, 499–511.
- Schertler, G.F.X.** (1998) *Structure of rhodopsin*. *Eye*, 12, 504–510.
- Sicard, G. and Holley, A.** (1984) *Receptor cell responses to odorants—similarities and differences among odorants*. *Brain Res.*, 292, 283–296.
- Singer, M.S.** (2000) *Analysis of the molecular basis for octanal interactions in the expressed rat 17 olfactory receptor*. *Chem. Senses*, 25, 155–165.
- Singer, M.S., Weisinger-Lewin, Y., Lancet, D. and Shepherd, G.M.** (1995a) *Positive selection moments identify potential functional residues in human olfactory receptors*. *Receptors Channels*, 4, 141–147.
- Singer, M.S., Oliveira L., Vriend, G. and Shepherd, G.M.** (1995b) *Potential ligand-binding residues in rat olfactory receptors identified by correlated mutation analysis*. *Receptors Channels*, 3, 89–95.
- Strader, C.D., Sigal, I.S. and Dixon R.A.F.** (1989) *Structural basis of beta-adrenergic receptor function*. *FASEB J.*, 3, 1825–1832.
- Trabanino, R.J., Hall, S.E., Vaidehi, N., Floriano, W.B. and Goddard, W.A., III** (2004) *First principles predictions of the structure and function of G-protein coupled receptors: validation for bovine rhodopsin*. *Biophys. J.*, 86, 1904–1921.
- Vaidehi, N., Jain, A. and Goddard, W.A., III** (1996) *Constant temperature constrained molecular dynamics: the Newton–Euler inverse mass operator method*. *J. Phys. Chem.*, 100, 10508.
- Vaidehi, N., Floriano, W.B., Trabanino, R., Hall, S.E., Freddolino, P., Choi, E.J., Zamanakos, G. and Goddard, W.A., II** (2002) *Prediction of structure and function of G protein-coupled receptors*. *Proc. Natl Acad. Sci. USA*, 99, 12622–12627.
- Vriend, G.** (1990) *WHAT IF: a molecular modeling and drug design program*. *J. Mol. Graph.*, 8, 52–56.
- Wetzel, C.H., Oles, M., Wellerdieck, C., Kuczkowiak, M., Gisselmann, G. and Hatt, H.** (1999) *Specificity and sensitivity of a human olfactory receptor functionally expressed in human embryonic kidney 293 cells and Xenopus Laevis oocytes*. *J. Neurosci.*, 19, 7426–7433.
- Zamanakos, G.** (2001) *A fast and accurate analytical method for the computation of solvent effects in molecular simulations*. PhD thesis, California Institute of Technology, Pasadena, CA.
- Zhao, H., Ivic, L., Otaki, J.M., Hashimoto, M., Mikoshiba, K. and Firestein, S.** (1998) *Functional expression of a mammalian odorant receptor*. *Science*, 279, 237–241.

Accepted June 17, 2004